



Article

Composition and Structural Characteristics of Coal Gasification Slag from Jinhua Furnace and Its Thermochemical Conversion Performance

Zitao Zhao ¹, Wenlong Mo ^{1,*}, Guihan Zhao ¹, Yingshuang Zhang ^{1,*}, Hao Guo ¹, Jun Feng ¹, Zhiqiang Yang ², Dong Wei ², Xing Fan ^{1,3} and Xian-Yong Wei ^{1,4}

¹ State Key Laboratory of Chemistry and Utilization of Carbon Based Energy Resources, Key Laboratory of Coal Clean Conversion & Chemical Engineering Process (Xinjiang Uyghur Autonomous Region), School of Chemical Engineering and Technology, Xinjiang University, Urumqi 830046, China; zhaozitao@stu.xju.edu.cn (Z.Z.); zhaoguihan@stu.xju.edu.cn (G.Z.); fanxing@sdust.edu.cn (X.F.); wei_xianyong@163.com (X.-Y.W.)

² Xinjiang Tianyehuihe New Material Co., Ltd., Shihezi 831700, China; 13579452475@163.com (Z.Y.); weidong5761@163.com (D.W.)

³ College of Chemical and Biological Engineering, Shandong University of Science and Technology, Qingdao 266590, China

⁴ Key Laboratory of Coal Processing and Efficient Utilization, Ministry of Education, China University of Mining and Technology, Xuzhou 221116, China

* Correspondence: mowenlong@xju.edu.cn (W.M.); yingshuangzhang90@163.com (Y.Z.)



Citation: Zhao, Z.; Mo, W.; Zhao, G.; Zhang, Y.; Guo, H.; Feng, J.; Yang, Z.; Wei, D.; Fan, X.; Wei, X.-Y. Composition and Structural Characteristics of Coal Gasification Slag from Jinhua Furnace and Its Thermochemical Conversion Performance. *Sustainability* **2024**, *16*, 5824. <https://doi.org/10.3390/su16145824>

Academic Editor: Yunan Chen

Received: 5 June 2024

Revised: 29 June 2024

Accepted: 5 July 2024

Published: 9 July 2024



Copyright: © 2024 by the authors. Licensee MDPI, Basel, Switzerland. This article is an open access article distributed under the terms and conditions of the Creative Commons Attribution (CC BY) license (<https://creativecommons.org/licenses/by/4.0/>).

1. Introduction

Coal serves as a fundamental energy source and an important industrial raw material in China. Coal gasification technology enables the clean and efficient utilization of coal, and has been widely applied in the coal chemical industry. Coal gasification technology refers to the conversion of solid fuel into syngas during a gasification process, which is a key technology in coal industries such as coal-to-hydrogen transfer, coal liquefaction and methanol synthesis [1]. The technology of coal gasification to synthesize combustible gas and coal-based chemicals has, to a certain extent, alleviated the problem of fossil energy in China that is rich in coal, poor in oil and contains less gas, and effectively guaranteed

the strategic security of Chinese energy [2,3]. However, a large amount of coal gasification slag (including fine slag FS and coarse slag CS, fly ash and bottom slag) is produced during coal gasification [4]. Until 2020, China has produced over 50 million tons of gasification slag, with over 90% being stacked in the open or disposed of in landfills [5–7]. Gasification slag contains a lot of water and ash; the water will penetrate the surface and pollute the land and water source, and the ash will pollute the air along with dust. In addition, landfill treatment is commonly used at present and occupies a large amount of land resources and has serious impacts on the ecological environment [8,9].

Coal gasification slag is mainly composed of Al_2O_3 , SiO_2 , CaO , Fe_2O_3 , carbon residue and other components, and can be utilized to produce building aggregates, cementing materials, ceramics, wall materials and non-burning bricks among other building materials [1,10–12]. Additionally, the inorganic minerals obtained from coal gasification slag can be enhanced to polymers to improve their mechanical, thermal, acoustic and flame-retardant properties [13]. Fang et al. [6] used gasification slag to prepare cement, which improved the hydration degree of a pure cement system. However, the carbon residue in coal gasification slag can affect the stability of building materials, and the loss on ignition of raw materials is strictly required when it is used to produce building materials [14]. The national standard (GB/T1596-2017, China) stipulates that the loss on ignition of fly ash for cement concrete should be less than 10%, and the standard (JC/T409-2016, China) stipulates that the loss on ignition of fly ash for silicate building products is less than 8%. On the other hand, the residual carbon after gasification has a high calorific value, large specific surface area and abundant pore size, which can be used to prepare carbon materials such as adsorbents, carriers and electrochemical transport media [14]. Xue et al. [15] used the gravity separation method to separate the residual carbon from the crude coal gasification slag and then used it as an adsorbent to adsorb trimethoprim and sulfamethoxazole, which had a good effect and certain economic and environmental benefits. Therefore, carbon-ash separation in gasification slag is an important aspect for achieving its high value-added utilization and large-scale consumption [1,5]. Due to the characteristics of low density and small particle size, coal gasification fine slag is often separated by flotation [16]. Xue et al. [17] added naphthenic acid (flotation agent) to reduce the amount of collector. Shi et al. [18] proposed the selective dispersion flocculation method and compared it with the traditional flotation process, showing that it increased the combustible recovery rate of fine slag by 10.4%. Therefore, before “carbon-ash separation”, it is necessary to understand the structure and composition characteristics of coal gasification slag, as well as the existence and form of the ash and carbon residues.

It is evident that the structural and compositional characteristics and reactivity of coal gasification slag are significantly influenced by the type of gasifier, gasification conditions and the type of coal. Hu Xiao-Bo et al. [19] from our research group analyzed the bottom slag and fly ash from a fluidized bed gasifier using high-alkaline coal from the Zhundong region. The results showed that the bottom slag had an ash content as high as 99%, while the carbon content and combustion performance of the fly ash were superior to the raw coal. After several years of research and verification by experts, fly ash was sold at USD 276 per ton (compared to USD 55 per ton for raw coal), and there was a high demand for it. The benefits of selling fly ash could offset all the costs of raw materials in the gasification process. Xu Xiaowei et al. [20] analyzed the coarse and fine slag from a Texaco gasifier based on high-alkaline coal from the Zhundong region in Xinjiang. They found that the weight loss rates during pyrolysis and combustion were higher for the coarse slag than for the fine slag, and that the relative content of aliphatic and aromatic functional groups in the coarse slag was higher.

The Jinhua furnace gasification process is characterized by its strong safety, high energy efficiency, rapid system startup, good stability and strong adaptability to various types of coal. This process, based on traditional coal–water slurry gasifiers, incorporates a waste heat recovery boiler to recover heat generated during gasification. This study focuses on the gasification residues (coarse and fine slag) from the Jinhua furnace process

of a company in Xinjiang (using Zhundong coal as raw material), analyzing their physical and chemical characteristics, including proximate analyses, ultimate analyses, surface morphology (SEM), crystal phase structure (XRD), ash composition (XRF) and functional group distribution (FT-IR). The relationship between the compositional and structural characteristics of the Jinhua furnace coal gasification slag and its pyrolysis and combustion reactivity is explored based on thermogravimetric behavior experiments (TG-DTG).

2. Materials and Methods

2.1. Materials

As shown in Figure 1, Jinhua furnace is mainly divided into gasification chamber and a heat recovery chamber, and its gasification parameters are described in detail in Table S1. In the process of coal gasification, raw coal (TYC), water and a limited quantity of additives are ground in the rod mill to make coal slurry with a concentration of about 61%, and the coal slurry enters the water wall gasifier through the process burner under the action of a high-pressure coal slurry pump. Oxygen from the air separation system enters the gasifier through the process burner, and reacts with the coal slurry in the gasification combustion chamber to produce water gas. The combustion chamber is equipped with a water-cooled wall type, and the heat recovery chamber is installed below the gasification chamber, which can recover the heat from the by-product steam. The crude syngas and molten slag generated in the combustion chamber are recovered by the radiation heat recovery chamber in the lower part of the gasifier during the descent process, and the high temperature and high-pressure steam are produced by the by-product. The cooled crude syngas enters the washing and purification system through the syngas pipeline. The cooled slag is periodically discharged into the slag tank through the slagging system to obtain coarse slag (CS). Crude syngas passes through Venturi scrubber, scrubber and four-stage flash successively to obtain clean syngas and black water (BW), and then the black water is settled and filtered to obtain gray water and fine slag (FS). Samples of TYC, FS and CS were taken and placed in a fume hood for drying under air atmosphere. After drying, samples were ground through a 60-mesh screen for use.

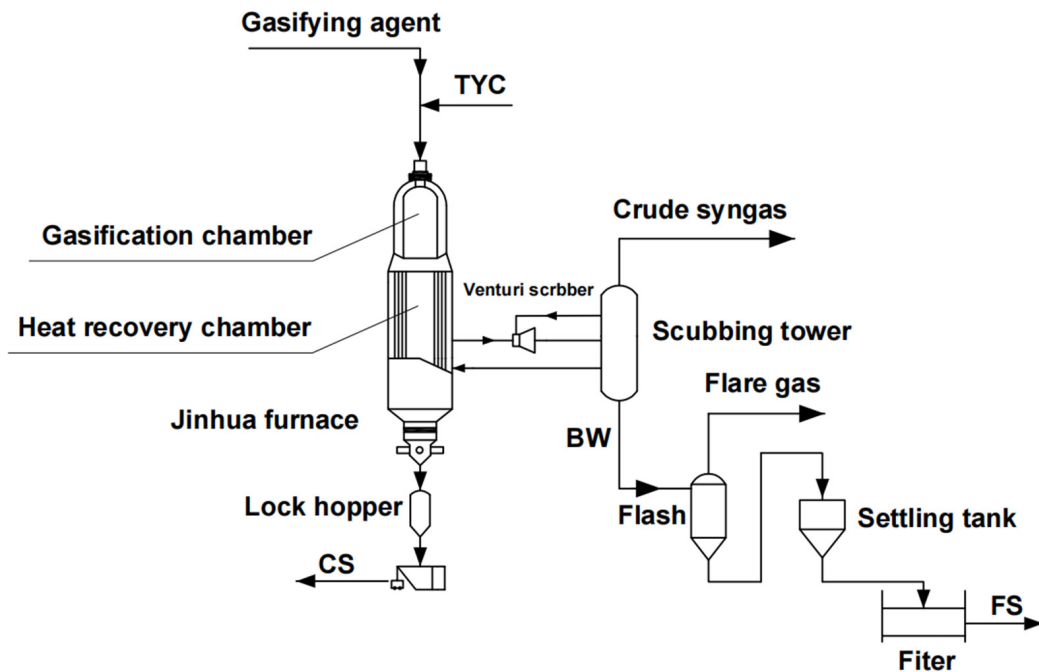


Figure 1. Diagram of Jinhua gasifier.

2.2. Analyses Methods

2.2.1. Proximate Analyses and Ultimate Analyses

According to GB/T212-91 (China), the moisture, ash and volatiles in the residue samples were analyzed, and the fixed carbon content was calculated. The contents of C, H, N and S elements were measured by the German Elementar UNICUBE element analyzer (Langenselbold, Hesse, Germany) and CHNS mode, and the O content was calculated by difference subtraction method.

2.2.2. Surface Properties Analyses

Scanning electron microscope–energy spectrometer (SEM-EDS, Sigma300, ZEISS, Jena, Germany) was used to analyze the surface morphology and elemental composition of the samples in different regions. Composition and chemical valence of the surface elements were tested by X-ray photoelectron spectroscopy (XPS, K-Alpha, Thermo Scientifi, Boston, MA, USA). The binding energy of O element was calibrated with reference to the C1s peak at 284.8 eV. The types and quantities of oxygen-containing and nitrogen-containing functional groups could be determined by fitting the sub-peak C1s. The pore structure on the surface of FS particles was analyzed by the automatic specific surface area and porosity analyzer (BET, ASAP2460, Micromeritic, Norcross, GA, USA). The test conditions of the analyzer are heating stage rate of 10 °C/min, degassing temperature of 90 °C, degassing time of 12 h, holding temperature of 200 °C, pressure of 100 mmHg.

2.2.3. Composition and Structure Characteristics Analyses

Functional group and structure types were analyzed using infrared spectroscopy (FTIR, Nicolet iS20, Thermo Scientific, Waltham, MA, USA). The composition of the ash sample was analyzed by X-ray fluorescence spectrometer (XRF, ZSX Primus III, Rigaku, The Woodlands, TX, USA). The crystal structure of the sample was characterized by X-ray diffractometer (XRD, D8 Advance, Bruker, Madison, WI, USA), and the XRD pattern was recorded by Cu K α (15 mA, 40 kV, K α = 0.15406 nm) radiation with a working range of 10–80° and step size 10°·min⁻¹. Jade 6.0 software was used to identify databases created by Powder Diffraction Standards (JCPDS).

2.2.4. Thermal Conversion Analyses

Thermogravimetric analyzer (TG, STA200, HITACHI, Tokyo, Japan) was used to test the pyrolysis and combustion characteristics of the samples from room temperature (25 °C) to 1000 °C with high-purity nitrogen and air, and the heating rate was 10 °C/min.

3. Results and Discussion

3.1. Proximate Analyses and Ultimate Analyses

Table 1 presents the results of proximate analyses and ultimate analyses of TYC, FS and CS. It is evident that the ash content in the three samples was high, especially the ash content in the CS which was as high as 98.07%, which is more suitable for inorganic materials. After TYC gasification, the volatile content of FS and CS decreased sharply, and the volatile content of CS was as low as 0.26%. It can be seen from the table that FS contains 35.82% fixed carbon and 59.34% ash, indicating that the important premise of its resource utilization is carbon–ash separation.

Table 1. Proximate and ultimate analyses (wt.%).

Sample	Proximate Analysis (ad, %)					Ultimate Analysis (daf, %)					H/C
	M	A	VM	FC	C	H	N	O _{diff}	S _{t,d}		
TYC	2.48	19.83	26.11	51.58	81.97	4.86	1.01	11.58	0.58	0.711	
FS	0.85	59.34	3.99	35.82	98.09	1.22	0.62	0.02	0.05	0.148	
CS	0	98.07	1.67	0.26	81.04	6.11	0	0.01	12.83	0.905	

ad: air dry base; diff: by difference subtraction calculation; daf: dry ash free base.

From the ultimate analysis, it is evident that the organic compounds TYC, FS and CS are mainly composed of C, H and O elements, accounting for about 90%, and the C content of FS is as high as 98.09% (daf), indicating that FS contains rich carbon components. At the same time, FS H/C decreased from 0.711 to 0.148 after gasification, which was attributed to the increase in the graphitization degree of the sample after gasification. In order to further explore the composition characteristics and resource utilization path of fine slag, the basic physical and chemical properties of FS, such as morphological characteristics, element distribution, pore structure and crystal composition, were analyzed by comparing it with raw coal, and the differences in thermochemical conversion performance between raw coal and FS were compared.

3.2. Surface Properties Analysis

3.2.1. Surface Morphology and Element Distribution

The surface micromorphology of TYC and FS at different scales is shown in Figure 2a–f. It can be seen that TYC is blocky or layered, with a flat, smooth surface and uniform texture, whereas FS is mainly divided into two morphologic types: loose, porous, flocculent and regular, smooth, spherical particles.

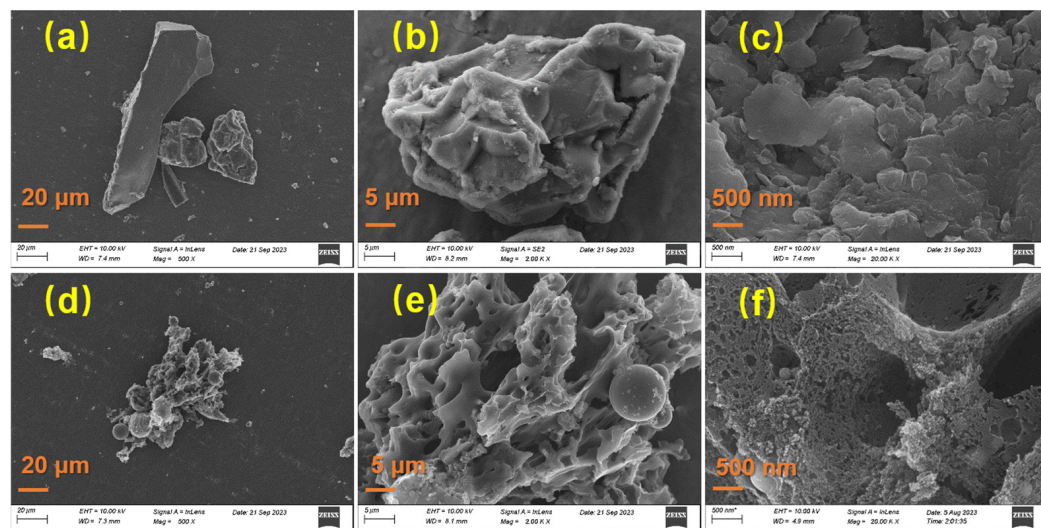


Figure 2. Scanning electron microscope images of TYC (a–c) and FS (d–f).

EDS was used to measure the element content of TYC and FS in different regions, as shown in Figure 3. As can be seen from the figure, there is little difference in the element content of TYC in different regions, while there is a significant difference in the element content of FS in flocculent and spherical particles, mainly in C, O and Si elements (35.76%, 45.1% and 18.89% in flocculent, and 4.93%, 59.13% and 35.79% in spherical particles, respectively). It shows that the residual carbon in FS is mainly present in the form of a flocculent, while the ash mainly presents in the form of regular smooth spherical particles. As shown in Figure 2f, the flocculent carbon residue of FS is inlaid with smaller scale ash-rich smooth spherical particles. The possible reason is that the critical viscosity temperature (T_{cv}) of non-crystalline glass slag in fine slag is low [10], coupled with the fact that the operating temperature of Jinhua furnace is 1600 °C. After the gasification of a coal water slurry and gasifier at high temperature, a lot of heat is generated, resulting in local heating of the surface of the carbon component and melting of the surrounding glass body. Under the action of the gasification agent, the molten amorphous particles (vitreous) are divided into spherical droplets of different sizes, which are cooled into spherical particles when passing through the heat recovery chamber and adhere to the pores of the residual carbon. At the same time, it could be seen that the amorphous vitreum (ash) and flocculent carbon

residue exist in the form of a coating by embedding or attaching to the surface of the pore of carbon residue or blocking the pores.

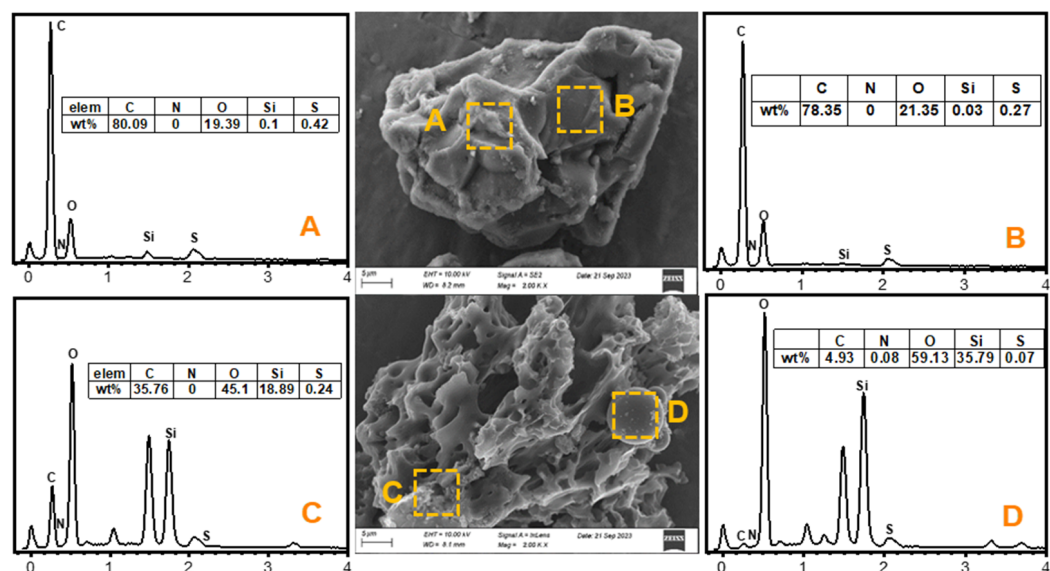


Figure 3. Surface morphology and elemental distribution of TYC and FS. A and B detailing the content for TYC and C and D for FS.

3.2.2. TYC and FS Surface Element Characteristics

Figure 4 shows the full XPS spectra of TYC and FS. The surfaces of TYC and FS are mainly composed of C, O, Si, Al and other elements, and the content of C element on the surface of TYC is higher than that on the surface of FS, which is consistent with the results obtained in Table 1. The amounts of Si, Al and other elements on the FS' surface were higher than those on the surface of TYC, which was caused by the adsorption of a large number of ash particles on the FS' surface. Figure 5 shows the C1s and O1s spectra of the TYC and FS' surfaces and their fitting curves. The distribution results of C and O elements are listed in Table 2. It can be seen from the table that the C 1s of TYC and FS mainly consist of $>\text{C}-\text{C}<$ (284.4 eV) and $>\text{C}-\text{H}$ (285.2 eV) structures. Among them, the gasification process increases the $>\text{C}-\text{C}<$ structure and decreases the $>\text{C}-\text{H}$ structure, resulting in the H/C in the elemental analysis in Table 1 dropping from 0.711 to 0.148. In addition, there was little difference in the content of $>\text{C}-\text{O}-$ (286.3 eV), $\text{C}=\text{O}$ (287.3 eV), $-\text{COO}-$ (288.6 eV) and $\pi-\pi^*$ (291.5 eV) between the two samples.

Table 2. Distribution of C and O forms in TYC and FS from analysis with XPS.

Elemental Peak	Functionality	Binding Energy (eV)	Molar Content (%)	
			FS	TYC
C 1s	$>\text{C}-\text{C}<$	284.4	64.14	49.73
	$>\text{C}-\text{H}$	285.2	28.13	41.42
	$>\text{C}-\text{O}-$	286.3	3.44	3.80
	$\text{C}=\text{O}$	287.3	1.98	2.40
	$-\text{COO}-$	288.6	1.64	1.67
	$\pi-\pi^*$	291.5	0.67	0.97
	$>\text{C}-\text{O}$	531.6	83.50	45.85
	$>\text{C}-\text{OH}$	532.4	11.99	35.55
	$>\text{C}-\text{O}-$	533.1	1.87	15.40
	$-\text{COOH}$	534.1	2.64	3.20

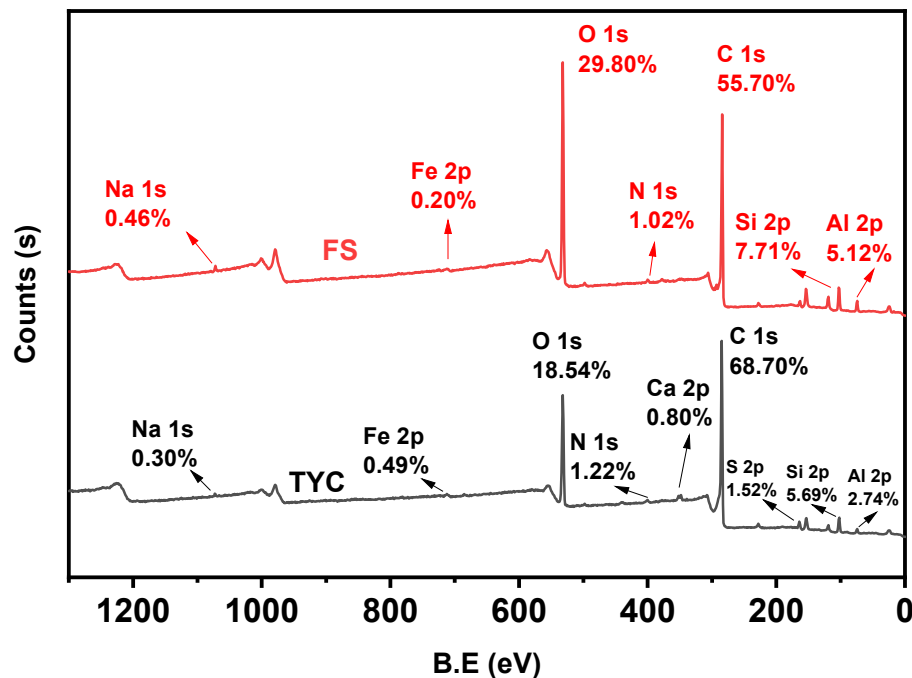


Figure 4. XPS profiles of TYC and FS.

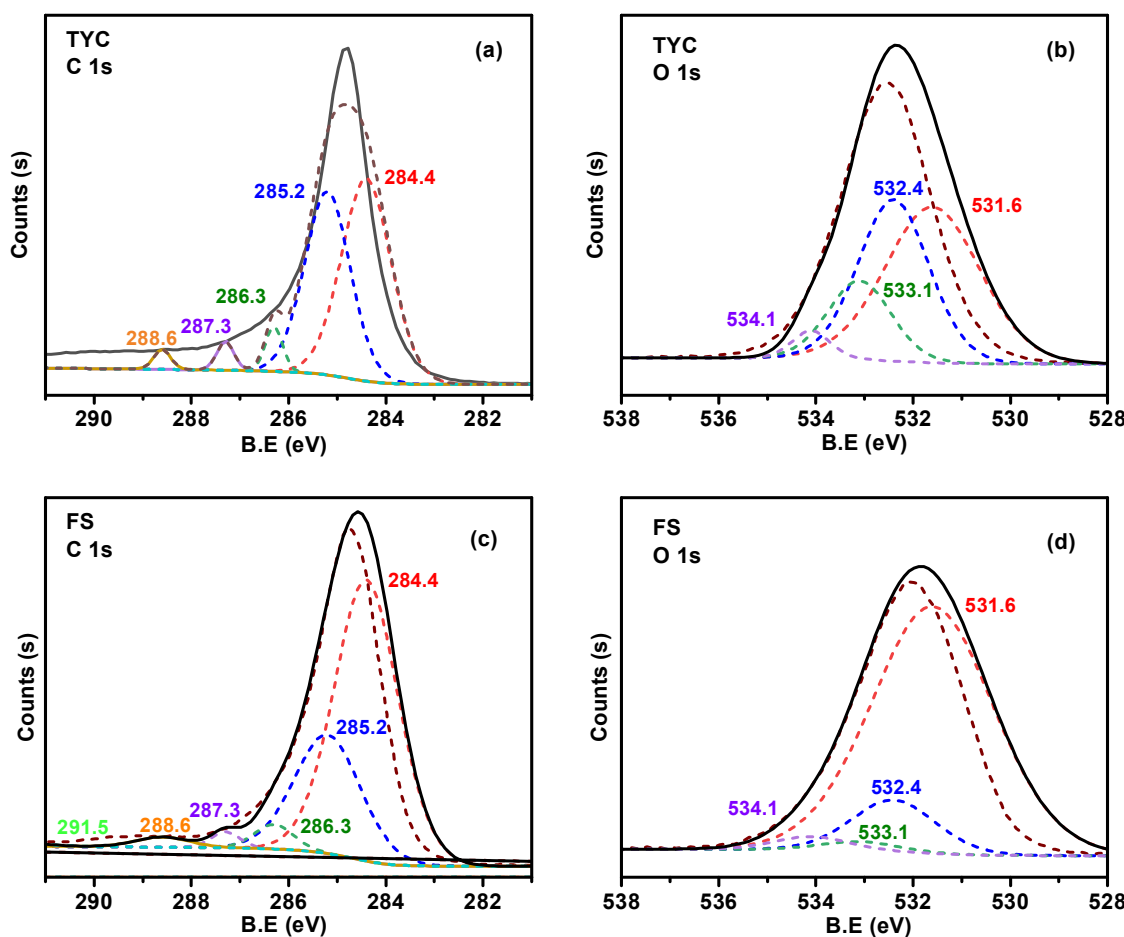


Figure 5. C 1s and O 1s spectra and their fitting curves of TYC and FS: (a) C 1s in TYC; (b) O 1s in TYC; (c) C 1s in FS; (d) O 1s in FS. The solid line represents the original curve, while the dashed line represents the fitted curve.

The surface O atomic contents of TYC and FS were 18.54% and 29.80%, respectively, which could be divided into four types: >C=O (531.6 eV), >C-OH (532.4 eV), >C-O- (533.1 eV) and -COOH (534.1 eV). It can be seen that the form of the O element in TYC is relatively rich, which is due to the high content of organic matter in TYC. However, after gasification, due to the rapid reduction in the FS' volatile content, FS mainly presents with a stable >C=O structure (83.50%). According to the forms of C and O distributed in the XPS atlas, there are hydrophilic oxygen-containing functional groups (C-O-C, -OH) and inorganic minerals on the surface of FS, which easily form hydrogen bonds with H₂O in the pulp and form hydration films on the surface of FS. FS can be considered for the preparation of coal water slurry to realize resource utilization.

3.2.3. Analyses of Specific Surface Area and Pore Size of FS

Based on the loose porous characteristics of FS in Figure 2, the BET (Brunauer–Emmett–Teller) model was used to calculate the specific surface area and pore volume of the gasification slag. The t-plot model was used to calculate the specific surface area and volume of micro-holes, and the results are shown in Table 3. It could be seen that the specific surface area of FS is 353 m²/g, the mesoporous pore volume is 0.35 cm³/g, and the average pore size is 3.95 nm, indicating that FS mainly presents in the form of mesopores. According to the large specific surface area of FS, adsorbents and other carbon materials can be made immediately or after the ash has been removed.

Table 3. Pore structure parameters of FS.

Sample	SSA _{BET} (m ² g ⁻¹)	TPV _{BJH} (cm ³ ·g ⁻¹)	ADM _{BJH} (nm)
FS	352	0.35	3.95

Figure 6a shows the N₂ adsorption/desorption isotherm of gasification slag. The figure reveals that the adsorption and desorption isotherm of the gasification slag in N₂ is a reversible “S”-shaped line, indicating that the gasification slag contains a relatively complete pore structure [21]. According to the classification of physical adsorption isotherm proposed by the IUPAC, the adsorption curve belongs to type II. As P/P₀ increases, N₂ adsorption transitions from monolayer to multilayer adsorption. When P/P₀ is greater than 0.4, the isotherm has a hysteresis ring, belonging to the H4 type, which is usually associated with capillary condensation of mesoporous structure. At relatively low pressures, the adsorption/desorption isotherms overlap, indicating the presence of many semi-open micropores in the sample.

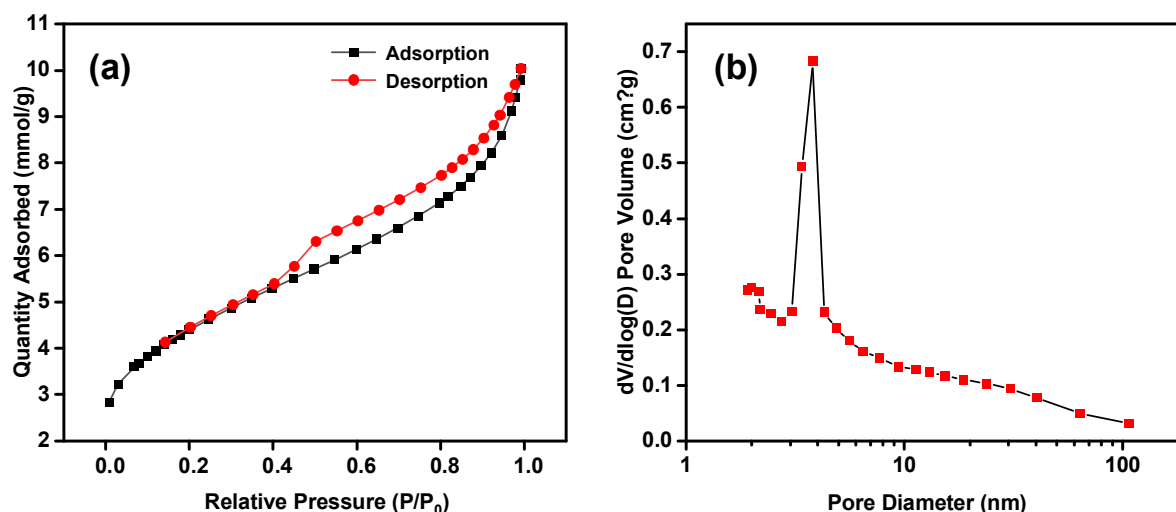


Figure 6. Adsorption and desorption curves (a) and pore size distribution (b) of TYC and FS.

Figure 6b further confirms the pore size distribution of gasification slag calculated by the BJH model, and the pore size is mainly concentrated at 3.77 nm. Concurrently, it indicates that there is a relatively complete porous structure in the gasification slag, and mesoporous pores are the main ones.

3.3. Composition and Structure Characteristics of Three Sample

3.3.1. FTIR

As shown in Figure 7, the absorption peaks of FS and CS were significantly lower than those of TYC, which was caused by the decomposition or transformation of organic components in large quantities during the gasification process of TYC. The vibration peak in TYC at 3695 cm^{-1} was attributed to the stretching vibration peak of metal hydroxide O-H, and the stretching vibration of crystal water at 3620 cm^{-1} was migrated to 3430 cm^{-1} after gasification, indicating that part of the -OH structure of TYC was decomposed into small molecules such as water molecules by heat [22]. An antisymmetric stretching vibration in the long chain alkyl at 2918 cm^{-1} and symmetric stretching vibration at 2850 cm^{-1} of TYC indicated that a long-chain alkyl existed in TYC and was arranged in an orderly manner, while no absorption peak was found in FS and CS in this band, indicating that most of -CH₂- have broken down during gasification, forming small molecules such as CO₂ and H₂ [21,23]. The symmetrical stretching vibrations in the aromatic C=C at 1590 cm^{-1} and ortho-substituted aromatic hydrocarbon (3H) at 798 cm^{-1} indicate the presence of aromatic compounds in TYC [20,22]. The absorption peak of about 1000 cm^{-1} is attributed to the amorphous crystal, corresponding to the asymmetric Si-O-Si and Si-O-(Al) stretching vibration, which is a typical amorphous silicaluminate structure [24].

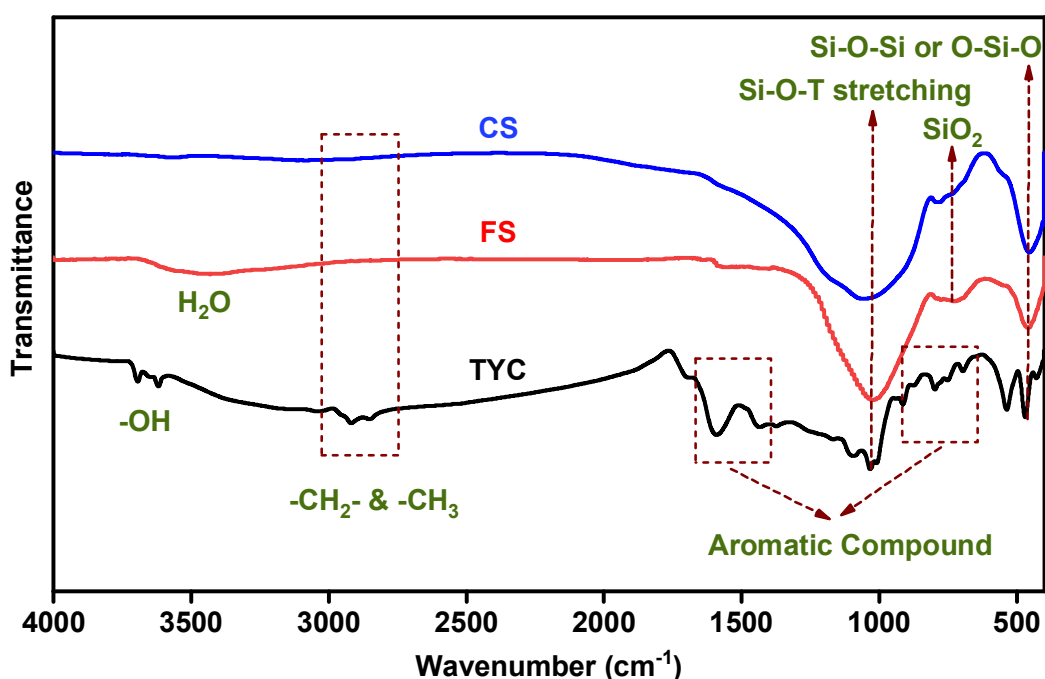


Figure 7. FT-IR spectra of TYC, FS and CS.

The vibration peak in FS at 3430 cm^{-1} is attributed to the stretching vibration of crystal water, indicating that there is crystal water in silicate and other clay minerals [21,22]. The banding in the range $950\text{--}1050\text{ cm}^{-1}$ is caused by the asymmetric tensile vibrations of the tetrahedron TO₄ (T for Si or Al) in Si-O-T in the geopolymers structure [24,25]. The absorption peaks of FS at 1022 cm^{-1} and CS at 1055 cm^{-1} are caused by the asymmetric vibrations of Si-O-Si and Si-O-Al in silica-aluminite minerals. The absorption peak at 789 cm^{-1} belongs to the characteristic peak of quartz [18]. The absorption peak of $400\text{--}500\text{ cm}^{-1}$ is caused by the flexural vibration of Si-O-Si or O-Si-O bonds, and there

are obvious absorption peaks in FS and CS, which is consistent with the high content of Al and Si in FS and CS and the rich crystals formed by them [24]. In summary, TYC contains aliphatic hydrocarbons, aromatic compounds, and a small number of inorganic components, whereas FS and CS are primarily composed of ash with a tetrahedral TO_4 framework (where T represents Si or Al). This is due to the fact that, during the coal gasification process, the organic components of TYC are decomposed into small molecular compounds and subsequently converted into synthesis gas. The ash undergoes a series of reactions internally at high temperatures, resulting in the formation of CS and FS.

3.3.2. Phase Analyses

The XRD patterns in Figure 8 show that the XRD patterns of TYC and FS are basically similar, with obvious SiO_2 peaks at $2\theta = 20\text{--}30^\circ$ and weak diffraction peaks of $\text{CaAl}_2\text{Si}_2\text{O}_8\text{H}_2\text{O}$ at $2\theta = 20.84^\circ$, 27.87° and 54.88° . In addition, CS has a wide variety of other crystal structures. It mainly includes SiO_2 (quartz), $\text{CaAl}_2\text{Si}_2\text{O}_8\text{H}_2\text{O}$ (anorthite), K_2SO_4 (potassium sulfate), $\text{Ca}_{1.5}\text{SiO}_{3.5}\text{H}_2\text{O}$ (calcium silicate), $\text{Ca}_2\text{Al}_2\text{SiO}_6(\text{OH})_2$ (kamaishilite), $\text{K}_2\text{Ca}_2(\text{SO}_4)_3$ (calcium potassium sulfate), $\text{Ca}_6\text{Si}_6\text{O}_{17}(\text{OH})_2$ (xonotlite), etc. In the process of TYC gasification, the amorphous glass slag in the ash easily forms a crystalline slag at high temperatures, which is discharged from the bottom of the furnace to form a coarse slag. The uncrystallized ash is carried out from the crude syngas and then goes through washing, flash evaporation, sedimentation and filtration to form FS.

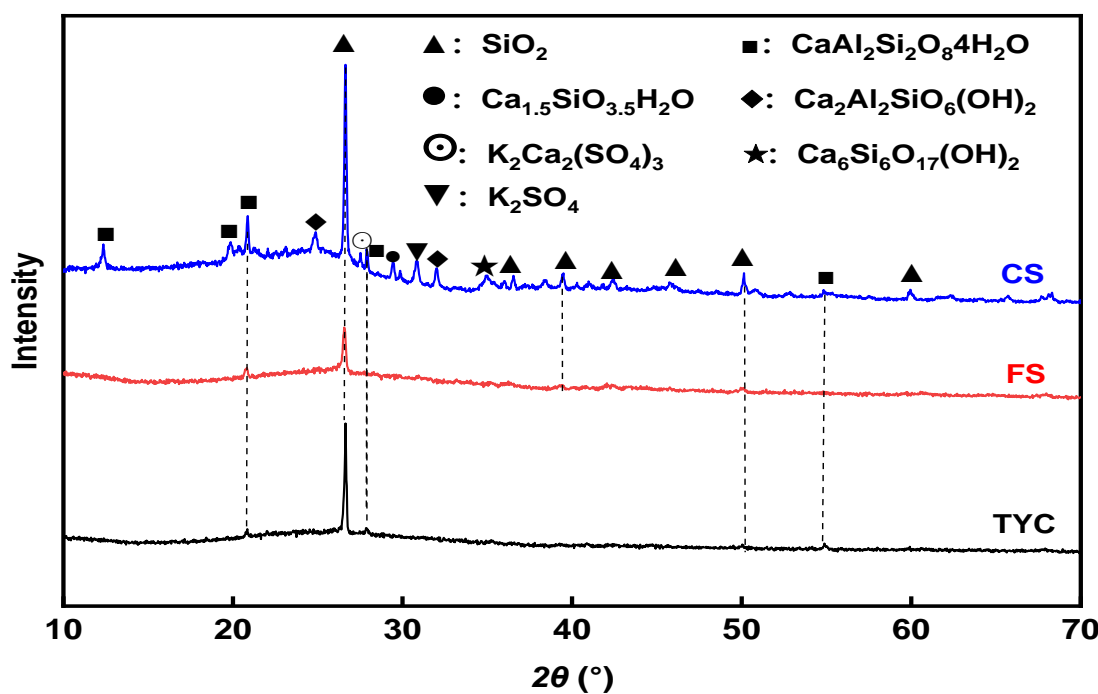


Figure 8. XRD spectra of TYC, FS and CS.

Table 4 shows the ash composition analyses of TYC, FS and CS. The main components are SiO_2 , Al_2O_3 , Fe_2O_3 and CaO , etc. CS and decarbonized FS can be used to make cement and iron-based catalysts [1]. The ash composition of the three samples primarily consists of acidic oxides (SiO_2 and SO_3), alkaline oxides (Fe_2O_3 , CaO , K_2O , MgO , TiO_2 and Na_2O) and amphoteric oxides (Al_2O_3). The amount of basic oxides and amphoteric oxides in FS is greater than CS, and the amount of acid oxides is less than in CS. Notably, the proportion of $\text{SiO}_2 + \text{Al}_2\text{O}_3$ in CS is close to 70%, and has a high Si/Al ratio, which can be considered for the preparation of porous materials such as molecular sieve.

Table 4. Ash composition (wt.%).

Sample	SiO ₂	Al ₂ O ₃	Fe ₂ O ₃	CaO	SO ₃	K ₂ O	MgO	TiO ₂	Na ₂ O	Other	SiO ₂ + Al ₂ O ₃
TYC	41.95	17.49	15.83	11.13	4.60	3.52	1.84	1.60	0.89	1.15	59.44
FS	43.04	21.29	14.10	9.63	1.21	3.03	2.81	1.29	2.25	1.35	64.33
CS	50.56	18.91	12.90	8.28	0.27	3.09	2.51	0.89	1.67	0.92	69.47

The content of basic oxides (especially trace oxides such as K₂O, Na₂O and TiO₂) and residual carbon can destroy the high-temperature network structure of the main crystalline components in coal gasification slag [10]. The sum of the contents of K₂O, Na₂O and TiO₂ in FS are greater than in CS (FS: 6.57%, CS: 5.65%) when combined with the fixed carbon content of FS in Table 1. It is inferred that CS is easier to crystallize when FS and CS pass through the heat recovery chamber after gasification. Acidic oxides, such as SiO₂, act as network formers, consisting of [SiO₄]⁴⁻ tetrahedrons and bridging oxygen bonds to form a three-dimensional interconnect network. Amphoteric oxide (Al₂O₃) acts as modifier or network formation according to the basicity of the slag. However, when one component changes, the impact of others is inevitable. TYC and FS in Figure 8 mainly consist of SiO₂ and CaAl₂Si₂O₈·4H₂O crystals, and the peak strength of TYC is greater than that of FS, indicating that the ash in TYC is divided into recombination components and light components due to changes in density and fluidization during gasification. The light component contains more K₂O, Na₂O, TiO₂ and other trace basic oxides, while the recombination component contains more SiO₂, etc., which easily form [SiO₄]⁴⁻ tetrahedron and make it easier to produce crystallization.

3.4. Thermal Conversion Performance of FS and TYC

3.4.1. Thermogravimetric Behavior in Inert Atmosphere

Figure 9 shows the TG and DTG curves of TYC and FS pyrolysis. As depicted in Figure 9a, the weight loss rates of TYC and FS were 27.49% and 10.38%, respectively, and the difference in weight loss rates was mainly attributed to the difference in volatile fractions. TYC reaches its peak weight loss rate at about 470 °C, while FS's weight loss rate is relatively gentle, and obvious weight loss occurs when it reaches 900 °C. According to Figure 9b, TYC has three obvious weight loss rate peaks, and the first peak appears at about 78 °C, which is caused by the escape of water in physical adsorption and other small molecules in TYC. The weight loss rate peak at around 470 °C is due to the breakdown of macromolecular network structure in coal and the breakdown of C-C bond on fat chain [26,27]. The weight loss peak after 600 °C is due to the condensation dehydrogenation reaction of aromatic structure and hydrogenated aromatic structure or the decomposition reaction of heterocyclic compounds [28]. For example, the weight loss rate peak of TYC at 714 °C is due to the generation of small molecules such as CO, H₂ and CH₄. FS has two peaks of 658 °C and 823 °C before 900 °C, but the peaks are weak. It is worth noting that after 900 °C, FS has an obvious peak. On the one hand, because the fine slag is mainly composed of amorphous glass, and the critical viscosity temperature (T_{CV}) of amorphous glass is low, the glass slag begins to decompose after 900 °C [10]. On the other hand, because there are more carbonates in the ash, the decomposition occurs after 900 °C to produce CO₂.

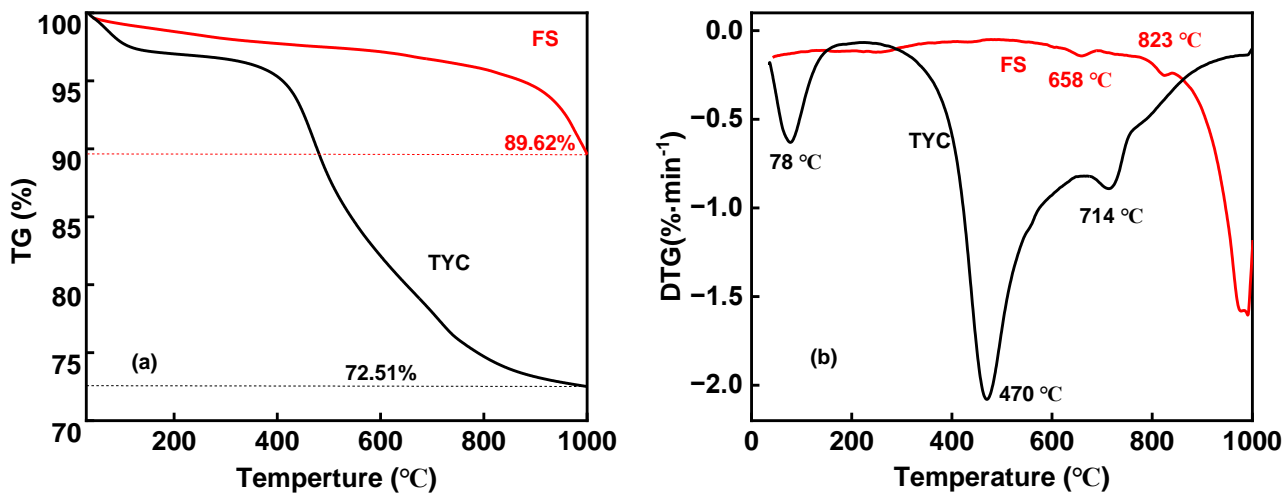


Figure 9. TGDTG profiles of TYC and FS under N_2 atmosphere: (a) TG; (b) DTG.

3.4.2. Thermogravimetric Behavior in Oxygen Atmosphere

Figure 10 shows the combustion TG and DTG curves of TYC and FS. In order to further compare the differences in combustion performance of the samples, the comprehensive combustion index S of the two samples was calculated according to the TG and DTG distributions, and the results were shown in Table 5. The comprehensive combustion index S reflects the comprehensive characteristics such as ignition temperature (T_i) and burnout temperature (T_f) of the two samples, and is determined using the following equation:

$$S = (DTG_mDTG_a)/(T_i^2 T_f)$$

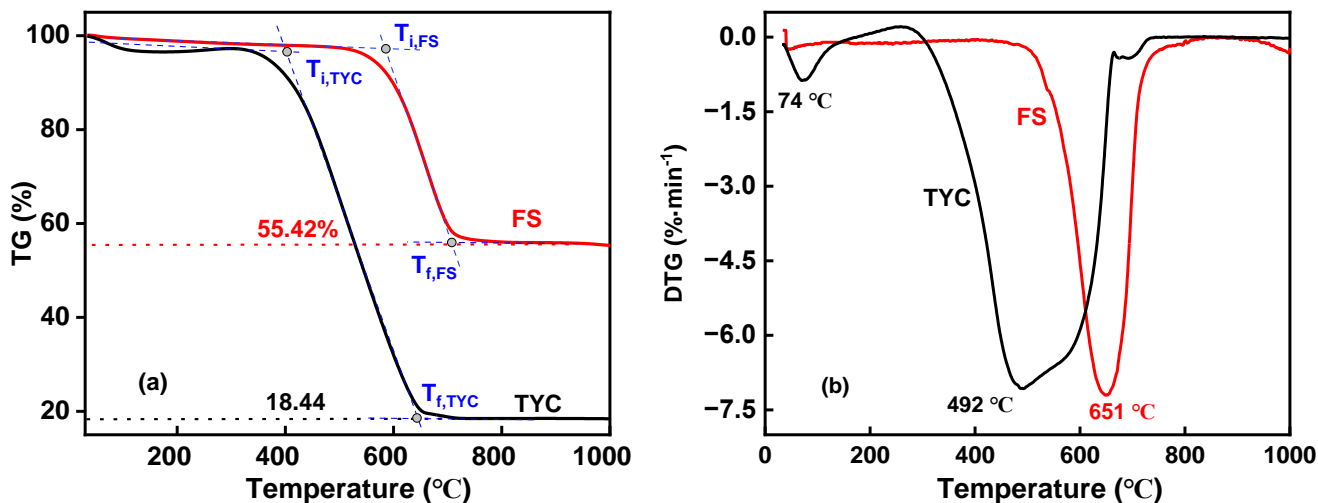


Figure 10. TGDTG profiles of TYC and FS under air atmosphere: (a) TG; (b) DTG.

Table 5. Combustion characteristic parameters of TYC and FS.

Sample	T_i (°C)	T_f (°C)	T_{max} (°C)	DTG_{max} (%/min)	DTG_{mean} (%/min)	S
TYC	402	645	492	-7.10	-1.69	1.15×10^{-7}
FS	586	707	651	-7.22	-0.93	3.01×10^{-8}

As can be seen from Figure 10a, the weight loss rates of TYC and FS were 81.69% and 44.40%, respectively, and can be attributed to the loss of water, volatiles and combustion of

fixed carbon. According to Figure 10b, TYC appeared a small peak at about 70 °C, mainly because the TYC contained a certain number of small molecules which escaped at this stage. The TYC displayed an obvious acromion in the main combustion stage (402–645 °C), indicating that the combustion mode of TYC was homogeneous to heterogeneous ignition, whereas FS lacked such an acromion in its main combustion stage, indicating that the combustion mode was homogeneous combustion [19]. It is worth noting that TYC showed a slight upward trend between 130 and 320 °C, which was similar to the Zhundong subbituminous coal reported by Xu Xiaowei et al. [20] and Hu Xiaobo et al. [19]. In this stage, >C-OH and -CHO in the coal may be oxidized into groups such as -COOH.

The comprehensive combustion index is presented in Table 5. The ignition temperature (T_i) of TYC is 402 °C, and the burnout temperature (T_f) is 645 °C, while the ignition temperature and burnout temperature of FS are higher than those of TYC, which may be due to its characteristics of high ash content, low volatile content and high degree of graphitization. The maximum weight loss rate peak temperature (T_{max}) of FS was 651 °C, significantly exceeding that of TYC. The maximum weight loss rate (DTG_{max}) of TYC is comparable to that of FS, while the average weight loss rate (DTG_{mean}) of TYC was about twice that of FS, and the comprehensive combustion index (S) was about 4 times that of FS. Clearly, the combustion performance of FS is worse than that of TYC, but the thermal stability of FS in air is better. The literature shows that the common ignition temperature of activated carbon is 530 °C, while that of FS is as high as 586 °C, indicating that the number of oxygen-containing functional groups in the FS with oxidation edge decreases after gasification [29]. In view of the large specific surface area and good thermal stability in the air, FS can be used to prepare high temperature resistant carbon materials.

4. Conclusions

In this paper, the composition and structure of the coal gasification slag from the Jinhua Furnace were analyzed in detail, and the thermal conversion properties of the two under inert and oxidizing atmospheres were investigated. After raw coal (TYC) is gasified in the Jinhua furnace, the coarse slag (CS) is mainly composed of ash, and the fine slag (FS) is mainly composed of ash and fixed carbon. Among them, the FS has a mainly flocculent porous structure, encapsulated by or embedded with regular spherical inorganic components of different sizes, with high specific surface areas (353 m²/g) and pore volumes (0.35 cm³/g), and the pore size distribution is mainly mesoporous. In addition, the degree of carbon graphitization in FS is higher. In terms of inorganic components, FS is mainly composed of amorphous glass slag, while the ash in CS is mainly crystal slag which has a wide variety of presentations. By comparing the ignition temperature (T_i), burnout temperature (T_f), comprehensive combustion index (S), and CO₂ gasification performance as shown in Figure S1 of TYC and FS, it was found that the thermal stability of FS was better than that of TYC. Combined with its large specific surface area, FS could be used to prepare high-temperature-resistant carbon materials.

Supplementary Materials: The following supporting information can be downloaded at: <https://www.mdpi.com/article/10.3390/su16145824/s1>, Figure S1. Gasification reactivity of TYC and FS; Table S1. Parameters of Jinhua furnace.

Author Contributions: Methodology, J.F. and X.-Y.W.; Investigation, Y.Z.; Data curation, H.G.; Writing—original draft, Z.Z.; Writing—review & editing, W.M. and G.Z.; Project administration, Z.Y., D.W. and X.F. All authors have read and agreed to the published version of the manuscript.

Funding: This research was funded by National Natural Science Foundation of China (22368045), Key Technologies and Engineering Applications of Carbon Neutrality in High Carbon Emission Industries in Xinjiang, and High Quality Development Special Project for Science and Technology Supporting Industry from Changji (2022Z04).

Institutional Review Board Statement: Not applicable.

Informed Consent Statement: Not applicable.

Data Availability Statement: The original contributions presented in the study are included in the article/Supplementary Material, further inquiries can be directed to the corresponding authors.

Acknowledgments: The authors acknowledge the Xinjiang University for providing the experimental platform, and the reviewers for their scientific comments and suggestions. The authors are grateful to Wenlong Mo for instructions on topic selection, and to Xinjiang Tianyehuihe New Materials Co., Ltd. for kindly providing the materials.

Conflicts of Interest: Authors Zhiqiang Yang and Dong Wei were employed by the company Xinjiang Tianyehuihe New material Co., Ltd. The remaining authors declare that the research was conducted in the absence of any commercial or financial relationships that could be construed as a potential conflicts of interest.

References

1. Fang, K.; Wang, D.; Gu, Y. Utilization of Gasification Coarse Slag Powder as Cement Partial Replacement: Hydration Kinetics Characteristics, Microstructure and Hardening Properties. *Materials* **2023**, *16*, 1922. [[CrossRef](#)]
2. Gao, J.; Su, W.; Wang, X.; Song, X.; Wang, J.; Yang, J.; Yu, G. Corrosion and degradation mechanisms of high chromia refractory bricks in an entrained-flow gasifier: Experimental and numerical analysis. *J. Mater. Res. Technol.* **2023**, *24*, 8754–8765. [[CrossRef](#)]
3. Chen, R.; Lv, F.; Bao, Y.; Chen, F.; Dou, T.; Tu, G. A Discussion on CO₂ Sequestration in the UCG Space Based upon the Review of the UCG Residue Physicochemical Properties. *Minerals* **2023**, *13*, 616. [[CrossRef](#)]
4. Guo, F.; Chen, L.; Li, Y.; Zhu, Y.; Jia, W.; Guo, Y.; Guo, S.; Zhang, Y.; Wu, J. Review on the attribute cognition and carbon-ash-water separation of coal gasification fine slag. *Sep. Purif. Technol.* **2023**, *320*, 124121. [[CrossRef](#)]
5. Niu, Y.; Xu, J.; Chen, L.; Guo, S.; Guo, F.; Zhang, Y.; Wu, J. Cyclic catalytic Fe-N doped composite particle electrodes derived from gasification fine slag for non-selective mineralization of organic wastewater. *Fuel* **2024**, *355*, 129449. [[CrossRef](#)]
6. Liu, F.; Niu, G.; Guo, W. A Study on the Sintering Mechanism of High-Strength Light Bricks Manufactured from Coal Gasification Slag. *Sustainability* **2023**, *15*, 4860. [[CrossRef](#)]
7. Zhao, X.; Yang, K.; Wei, Z.; He, X.; Chen, R. Study on the effect of multi-source solid waste on the performance of its backfill slurry. *Heliyon* **2023**, *9*, e16251. [[CrossRef](#)]
8. Wang, H.; Chen, D.; Guo, R.; Tian, J.; Li, B. A Preliminary Study on the Improvement of Gangue/Tailing Cemented Fill by Bentonite: Flow Properties, Mechanical Properties and Permeability. *Materials* **2023**, *16*, 6802. [[CrossRef](#)] [[PubMed](#)]
9. Huo, B.; Zhang, J.; Li, M.; Zhou, N.; Qiu, X.; Fang, K.; Wang, X. Effect of CO₂ Mineralization on the Composition of Alkali-Activated Backfill Material with Different Coal-Based Solid Wastes. *Sustainability* **2023**, *15*, 4933. [[CrossRef](#)]
10. Listiyowati, L.N.; Santoso, I.; Sanwani, E.; Mubarok, M.Z. Effect of Minor Oxide and Residual Carbon on Coal Ash Crystallization Behavior and Slag Properties during Coal Gasification: Critical Literature Review and Thermodynamic Simulation. *ACS Omega* **2023**, *8*, 38794–38805. [[CrossRef](#)]
11. Guo, J.; He, C.; Yuan, M.; Fan, F.; Qin, Y.; Yan, J. Solid Precipitation Behaviors in Coal Slag from Different Primary Phases and Their Effects on Slag Viscosity from Thermochemistry and Experimental. *Processes* **2023**, *11*, 1522. [[CrossRef](#)]
12. Liu, K.; Yuan, Z.; Shi, C.; Zhao, H.; Wang, H. Effect of CaO-SiO₂-FeO slag system on coal gasification reaction in CO₂-Ar atmosphere and kinetic analysis. *J. CO₂ Util.* **2022**, *56*, 101850. [[CrossRef](#)]
13. Li, K.; Teng, Y.; Wang, K.; Chen, L.; Xue, C.-G. Mechanical activation of coal gasification fine slag and mechanical and thermal properties of coal gasification fine slag-poly(vinyl chloride) composites. *Mater. Res. Express* **2023**, *10*, 095301. [[CrossRef](#)]
14. Chen, C.; Sasaki, K.; Tian, Q.; Zhang, H. Effect of Alkali Fusion Methods on the Preparation of One-Part Geopolymer from Coal Gasification Slag. *ACS Omega* **2023**, *8*, 39366–39375. [[CrossRef](#)]
15. Xue, Z.; Feng, Y.; Li, H.; Xu, C.; Ju, J.; Dong, L.; Yang, C.; Bao, W.; Wang, J.; Wang, H.; et al. Adsorption of trimethoprim and sulfamethoxazole using residual carbon from coal gasification slag: Behavior, mechanism and cost-benefit analysis. *Fuel* **2023**, *348*, 128508. [[CrossRef](#)]
16. Chen, R.; Wang, H.; Li, D.; Liao, Y.; Tian, Q.; Su, W.; Li, L.; Zhang, H. Numerical and Experimental Study on the Colliding Flow Pulp Conditioning for the Separation Intensification of Unburned Carbon from Coal Gasification Slag. *Minerals* **2023**, *13*, 398. [[CrossRef](#)]
17. Xue, Z.-H.; Dong, L.-P.; Li, H.-P.; Fan, M.-Q.; Ren, Z.-Y.; Liu, A.; Fan, P.-P.; Bao, W.-R. Study on the mechanism of flotation of coal gasification fine slag reinforced with naphthenic acids. *Fuel* **2022**, *324*, 124557. [[CrossRef](#)]
18. Shi, D.; Zhang, J.; Li, H.; Li, S.; He, F.; Qu, J.; Chang, R.; Zhu, G.; Yang, C.; Wang, C. Insight into the mechanism of gasification fine slag enhanced flotation with selective dispersion flocculation. *Fuel* **2023**, *336*, 127134. [[CrossRef](#)]
19. Hu, X.; Yang, X.; Mo, W.; Zhang, S.; Ji, G.; Wei, X.; Xing, F. Structural characteristics and thermal conversion performance of ash and slag from circulating fluidized bed gasifier. *J. Fuel Chem. Technol.* **2022**, *50*, 1361–1370. [[CrossRef](#)]
20. Xu, X.; Mo, W.; Hao, C.; Liu, Y.; Wei, X.; Yang, X.; Zhang, S. Ash composition, structural characteristics and thermal conversion performance of Texaco gasifier based on Zhundong coal. *J. Fuel Chem. Technol.* **2022**, *50*, 777–786. [[CrossRef](#)]
21. Shen, H.; Fang, B.; Yan, K.; Qin, Y.; Wei, Y.; He, C. Oxygen vacancy-promoter on flotation residue carbon from coal gasification fine slag for the catalytic degradation of phenol. *Process Saf. Environ. Prot.* **2024**, *185*, 864–875. [[CrossRef](#)]

22. Tang, B.; Sun, Z.; Men, X.; Dong, K.; Wang, J.; Kong, L.; Bai, Y.; Guo, F. Synthesis of porous carbon/zeolite composites by low-temperature acid-alkaline leaching from coal gasification fine slag for adsorption of dye wastewater. *J. Environ. Chem. Eng.* **2024**, *12*, 112819. [[CrossRef](#)]
23. Cingo, X.; Nqombolo, A.; Mpupa, A.; Nyaba, L.; Mapazi, O.; Nomngongo, P.N. Valorisation of coal gasification slag and fly ash to mesoporous activated carbon @zeolite socony mobil-5 composite for preconcentration of pharmaceuticals and their removal. *Arab. J. Chem.* **2024**, *17*, 105838. [[CrossRef](#)]
24. Chen, C.; Shenoy, S.; Pan, Y.; Sasaki, K.; Tian, Q.; Zhang, H. Mechanical activation of coal gasification slag for one-part geopolymersynthesis by alkali fusion and component additive method. *Constr. Build. Mater.* **2024**, *411*, 134585. [[CrossRef](#)]
25. Qu, J.; Zhang, J.; Li, H.; Li, S.; Hou, X.; Chang, R.; Zhang, Y. Coal gasification slag-derived highly reactive silica for high modulus sodium silicate synthesis: Process and mechanism. *Chem. Eng. J.* **2024**, *479*, 147771. [[CrossRef](#)]
26. Fan, D.; Zhu, Z.; Lu, Q. TG-MS study on gas release characteristic during pyrolysis of bituminous coal. *Coal Convers.* **2014**, *37*, 5–10.
27. Zhao, Y.; Hu, H.; Jin, L.; He, X.; Wu, B. Pyrolysis behavior of vitrinite and inertinite from Chinese Pingshuo coal by TG-MS and in a fixed bed reactor. *Fuel Process. Technol.* **2011**, *92*, 780–786. [[CrossRef](#)]
28. Pan, C.; Liu, X.; Huo, W.; Guo, X.; Xin, G. Functional groups and pyrolysis characteristics of fine gasification ashes and raw coals. *CIESC J.* **2015**, *66*, 1449–1458.
29. Sádovská, G.; Honcová, P.; Morávková, J.; Jirka, I.; Vorokhta, M.; Pilař, R.; Rathouský, J.; Kaucký, D.; Mikysková, E.; Sazama, P. The thermal stability of carbon materials in the air: Quantitative structural investigation of thermal stability of carbon materials in air. *Carbon* **2023**, *206*, 211–225. [[CrossRef](#)]

Disclaimer/Publisher’s Note: The statements, opinions and data contained in all publications are solely those of the individual author(s) and contributor(s) and not of MDPI and/or the editor(s). MDPI and/or the editor(s) disclaim responsibility for any injury to people or property resulting from any ideas, methods, instructions or products referred to in the content.